

# INTERCOMPARISON OF INDUCED FIELDS IN JAPANESE MALE MODEL FOR ELF MAGNETIC FIELD EXPOSURES –EFFECT OF DIFFERENT COMPUTATIONAL METHODS AND CODES-

Akimasa Hirata<sup>1,\*</sup>, Kenichi Yamazaki<sup>2</sup>, Shoji Hamada<sup>3</sup>, Yoshitsugu Kamimura<sup>4</sup>, Hiroo Tarao<sup>5</sup>, Kanako Wake<sup>6</sup>, Yukihiisa Suzuki<sup>7</sup>, Noriyuki Hayashi<sup>8</sup>, Osamu Fujiwara<sup>1</sup>

<sup>1</sup>Nagoya Institute of Technology, Department of Computer Science and Engineering, Japan

<sup>2</sup>Central Research Institute of Electric Power Industry, Japan

<sup>3</sup>Kyoto University, Department of Electrical Engineering, Japan

<sup>4</sup>Utsunomiya University, Department of Information Science, Japan

<sup>5</sup>Takamatsu National College of Technology, Department of Electrical and Computer Engineering, Japan

<sup>6</sup>National Institute of Information and Communications Technology, EMC Group, Japan

<sup>7</sup>Tokyo Metropolitan University, Department of Electrical and Electronic Engineering, Japan

<sup>8</sup>Kyushu University, Department of Applied Science for Electronics and Materials, Japan

Received August 18 2009, amended month date year, accepted month date year

**Abstract** The present study provides an intercomparison of the induced quantities in a human model for uniform magnetic field exposures at extremely low frequency. A total of six research groups have cooperated in this joint intercomparison study. The computational conditions and numeric human phantom including the conductivity of tissue were set identically to focus on the uncertainty in computed fields. Differences in the maximal and 99th percentile value of the *in-situ* electric field were less than 30% and 10% except for the results of one group. Differences in current density averaged over 1 cm<sup>2</sup> of the central nerve tissue are 10% or less except for the results of one group. This comparison suggests that the computational uncertainty of the *in-situ* electric field/current density due to different methods and coding is smaller than that caused by different human phantoms and the conductivities of tissue, which was reported in a previous study.

## INTRODUCTION

There has been increasing public concern regarding the adverse health effects due to electromagnetic fields. Safety guidelines/standards for electromagnetic field exposures have been established by international standardization bodies (e.g., [1], [2]). According to the ICNIRP guidelines [1], together with related documents [3], the dominant effect of extremely-low frequency (ELF) fields on humans is caused by induced current, especially in the central nervous system (CNS). Current density averaged over an area of 1 cm<sup>2</sup> for the CNS tissue is used as a metric of basic restriction. The limit is 10 mA/m<sup>2</sup> for occupational exposure and 2 mA/m<sup>2</sup> for general public exposure at frequencies below 1 kHz [1]. Recently, attention has also been drawn to the *in-situ* electric field. One of the main reasons for this increasing attention is that the IEEE standards [2] used the *in-situ* electric field averaged over a straight line segment of 5 mm as a metric for human protection. Also of note is that the *in-situ* electric field has been reported to be a measure that is

relatively insensitive to tissue conductivity as compared to the induced current density [4].

Computational dosimetry in anatomically based numeric human body phantoms for magnetic field exposures has been conducted from the 1990s, especially at the University of Utah [5] and the University of Victoria [6], [7]. The resolutions of their numeric human phantoms were 7.2 mm and 6 mm, respectively, which are not sufficient to represent induced quantities in the CNS. As computational techniques the impedance method and the scalar potential finite difference (SPFD) method were used at the above universities. The conductivities used by these two groups were also different. In order to obtain insights on these differences, the University of Victoria and the University of Utah conducted intercomparisons of induced quantities [8], together with the data reported by the National Radiological Protection Board (NRPB, now named Health Protection Agency) [9]. One of the other motivations of such kind of studies is that there exists no analytical solution when considering anatomically-based model. The tissue or organ-averaged electric field/current density and the maximum induced current density were used as measures for comparison. Qualitative explanations from their differences were then given. The above measures, however, do not match the recent interest in

---

\*Corresponding author: Akimasa Hirata  
ahirata@nitech.ac.jp

the guidelines at ELF. The relative differences reported in [8] were more than a few hundred percent for several conditions and/or measures. A recent review of this topic has suggested a similar conclusion [10].

In recent years, anatomically based human phantoms with finer resolution are often used in computational dosimetry, in accordance with the development of computational resources [9, 11, 12, 13, 14, 15, 16, 17, 18]. The dosimetric measures to which attention was paid are induced current density averaged over an area of 1 cm<sup>2</sup> for CNS tissues and the 99th percentile value of the *in-situ* electric field, which are used in the environmental health criteria published by the World Health Organization [19]. The effect of (A) computational method, (B) human body model, and (C) conductivities of tissues on the dosimetric measures cannot be neglected, as is shown in [8].

In the present study, we focus on term (A), and then discuss the uncertainty in induced quantities by comparing the computational results calculated by six groups in Japan. The reason for focusing on term (A) is: The anatomically-based male adult phantom named TARO developed principally at the National Institute of Information and Communications Technology (NICT) is useful for gaining fundamental insight on this topic, since the model was developed based on a Japanese adult male with average height and weight [20]. The conductivities reported in [21] is used, since no further reliable data have been available this moment. The effect of different models on the dosimetric measure has been discussed in [18].

## MODEL AND METHODS

### Human Body Phantom

A whole-body numeric phantom for a Japanese male named TARO was developed by Nagaoka *et al.* [20]. The average height and weight of Japanese 18 to 30-year-olds are 1.714 m and 63.3 kg, respectively, for males. A volunteer was selected whose dimensions were close to the average values. The male volunteer was 22-years old, 1.73 m tall and weighed 65 kg. The resolution of the developed phantom is 2 mm and segmented into 51 anatomic regions. The height and weight of TARO are 1.73 m and 65 kg, respectively.

### Conductivities of Tissues

Table 1 shows the conductivity of body tissues used in the present study. These values were determined based on the report in [21]. The effect of permittivity of tissues on induced quantities in the ELF region is marginal since the conduction current is dominant as

Table 1. Conductivity of human tissues at 50 Hz determined by Gabriel (1996). \* represents central nervous tissues classified here for TARO.

Tissues	S/m	Tissues	S/m
cerebellum *	0.10	pancreas	0.35
C.S.F.	2.00	prostate	0.40
cornea	0.40	small intestine	0.50
eye humor	1.50	spleen	0.10
grey matter *	0.10	stomach	0.50
hypothalamus *	0.08	stomach contents	0.35
eye lens	0.25	tendon	0.30
pineal body*	0.08	testis	0.35
pituitary *	0.08	thyroid gland	0.50
salivary gland	0.35	trachea	0.35
thalamus *	0.08	urine	0.70
tongue	0.30	blood	0.70
white matter*	0.06	cortical bone	0.02
adrenals	0.35	bone marrow	0.06
bladder	0.20	cartilage	0.18
large intestine	0.10	fat	0.04
duodenum	0.50	muscle	0.35
esophagus	0.50	nerve (spinal cord)*	0.03
bile	1.40	skin	0.10
gall bladder	0.20	tooth	0.02
heart	0.10	ligament	0.30
kidney	0.10	diaphragm	0.35
liver	0.07	seminal vesicle	0.35
lung	0.14	cavernous body	0.35
large intestine contents	0.35	small intestine contents	0.35

compared to the displacement current. Thus, the permittivity of tissues is not considered in our computation.

### Computational Methods

Four different computational methods were used by different groups: the impedance method [22] at the Central Research Institute of Electric Power Industry (CRIEPI) [18] and NICT [17], a SPFD method [6] at Utsunomiya University (UU) [15] and Takamatsu National College of Technology (TNCT) [10], a fast-multipole surface-charge-simulation method for voxel data at Kyoto University (KU) [12], and quasi-static finite-difference time-domain method [23] at Nagoya Institute of Technology (NIT) [18]. Some in-house modifications and/or improvements have been implemented by each group. The validity of these computational codes has been confirmed for

homogeneous and/or multi-layer spheres. Some groups have presented their validation in a Technical Report by the Institute of Electrical Engineers of Japan (IEEJ) [24]. These four computational methods are briefly explained below.

#### *Impedance Method*

The impedance method solves a circuit network equation that represents a human body consisting of voxels having resistances. The human phantom was modeled by a number of voxels having conductivity  $\sigma$ , impedance  $Z$  at the side of the voxels, and loop current  $I$  on the surface of the voxels. The value of impedance  $Z$  at a side was defined by averaging the impedances of the four adjacent voxels sharing the corresponding side. According to Faraday's law, electromotive force  $V$  is induced on a surface of a voxel by the magnetic field. Using the impedance  $Z$  and loop current  $I$  (unknowns), closed loop equations are generated and solved simultaneously to obtain each loop current  $I$ . The four loop currents sharing the same side are then added to generate the current in each cell. Currents were defined at the center of each cell and obtained as the average of the four currents at the side having the same direction, and then the current density was obtained by dividing the current by the cross-sectional area of the voxel. In addition, the induced electric field was obtained by dividing the value of the induced current density by the conductivity  $\sigma$  of the voxel. A successive over-relaxation (SOR) method was adopted to solve the simultaneous equations.

#### *Scalar Potential Finite Difference Method*

This method is similar to the impedance method, and sets the branch current instead of the loop current. Defining scalar potentials (unknowns) at each node of a voxel, a branch current flowing from one node to a neighboring one along the side of voxels is derived, which includes a vector potential due to the applied magnetic fields and impedance between the nodes. By applying Kirchhoff's current law at all nodes, simultaneous equations are then set. The potential is solved iteratively using the SOR method. The electric field along the side of the voxel is obtained by dividing the difference of the potentials between nodes of the voxel by the distance across the nodes and adding the vector potential. The current density is obtained by multiplying the electric field with the average conductivity of the four adjacent voxels. Furthermore, the current density at the center of each voxel can be obtained in the same manner as in the impedance method.

#### *Quasi-static FDTD Method*

This method extends the conventional FDTD method to solve quasistatic problems by choosing incident waveforms appropriately. Under quasistatic approximation, fields exterior to conductors have the same phase as the incident field. The interior fields, on the other hand, are first-order fields that are proportional to the time derivative of the incident field. The incident field is then chosen as a ramp function, as in [23]. In order to generate a uniform magnetic field, two plane waves in opposite directions were excited so that the electric fields of the plane waves canceled each other out. The computed *in-situ* electric field can be linearly scaled to the target frequency.

#### *Fast-multipole surface-charge-simulation method for voxel data*

The surface-charge- simulation method is also called the indirect boundary element method. It solves the Laplace field that satisfies boundary conditions by superimposing partial fields caused by fictitious surface charges defined on the boundary elements. A square voxel facet having different conductivities on the face and back is defined as a boundary surface element. The boundary equation of current flux continuity through each surface element is expressed in an integral form based on the method of moment. To solve boundary equations for the unknown charge densities, an iterative solver, the Bi-CGsafe method in this analysis, is utilized. In order to speed up the iterative solver, and to reduce the required amount of memory, the fast multipole method in diagonal form [25] is applied. It should be noted that the number of surface elements defined in the TARO model was 3,921,953.

### **Computational Scenarios and Dosimetric Measures**

The numeric human phantom was considered to be standing in free space. Three orientations of uniform magnetic fields were considered as shown in Fig. 1; AP (front-to-back), TOP (top-to-bottom), and LAT (side-to-side). The frequency and amplitude of the magnetic field is chosen as 50 Hz and 0.1 mT, respectively.

We chose six measures for comparing the *in-situ* electric field and current density among the six research groups. For the electric field, we considered the following three measures: i) the maximum, ii) the 99th percentile one-voxel value of the *in-situ* electric field in the whole body phantom, and iii) the 99th percentile one-voxel values of the *in-situ* electric field for the respective CNS tissues. For the induced current, we considered the following three measures: iv) the

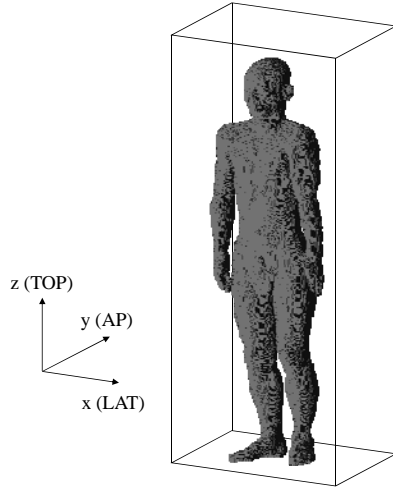


Fig. 1. Anatomically based Japanese adult male model and three exposure directions.

maximum one-voxel value of the current density in the whole body phantom and the maximum value of the current density averaged over an area of  $1 \text{ cm}^2$  in v) the whole body phantom and for vi) the CNS tissues.

The procedure for calculating the average current density is not defined in the ICNIRP guidelines [1]. The current density perpendicular to the three Cartesian planes is averaged over  $5 \times 5$  cells ( $1 \text{ cm}^2$ ). The magnitude of the current density is obtained using the three components of the  $1\text{-cm}^2$ -average current density [26]. When the air voxels were included in the averaging region, we performed the averaging without considering the air voxels. Note that the area of the air is not taken into account in the averaging procedure. When non-CNS tissues are included in the averaging region, the current densities in these tissues are considered based on the response of ICNIRP to CENELEC, which suggests that for the purpose of simplification, it is acceptable to assume that the  $1\text{-cm}^2$  sections are composed entirely of nervous tissue [26].

## COMPUTATIONAL RESULTS

Table 2 shows the computational results calculated by the six groups. As seen in Table 2, the difference in the current densities between TNCT and the other groups cannot be neglected while the *in-situ* electric fields are in good agreement. Similarly, the differences of the *in-situ* electric field obtained at CRIEPI and the remaining groups are significant, while those of current densities at CRIEPI are in reasonable agreement.

To gain insight into this difference, let us discuss the induced quantities calculated with the same method.

The mean difference in the *in-situ* electric field between CRIEPI and NICT for nine sets of data ((i), ii), and iii) for three exposure directions) was 60.4%, against 25.1% for the nine sets of data for the current density (iv), v), and vi) for three exposure directions). A possible reason for this is a computational convergence of the local electric fields, which may be attributed to the computation scheme of the determinant of the matrix, since the accuracy of the computational method with a matrix depends on how to solve the matrix. Note that the computational code of CRIEPI was shown to provide good accuracy for homogeneous and multilayer spheres [17].

Similarly, in the averaged difference for nine sets of data for the *in-situ* electric field between TNCT and UU, the mean difference between these two groups was 10.6%, while the difference was 46.5% for the nine sets of data. One possible reason for this difference could be the relative position assignment of the voxel and conductivity, which are different from the conventional SPFD method. This assignment may cause a higher difference in electrical conductivities at the tissue boundary, leading to computational uncertainty. Dealing with the conductivity in the SPFD method developed at TNCT is a task for forthcoming study.

In the following discussion, the reference value  $A_r$  is introduced as a mean value of the four groups excluding the maximum and minimum values provided by two groups. The difference  $D$  between the reference value and a result calculated by either one of the groups is defined by the following equation:

$$D = \frac{|A_r - A_i|}{A_r} \quad (1)$$

where subscripts  $r$  and  $i$  correspond to the data for the reference value and that obtained by a group.  $A$  is one of the six dosimetric measures defined above.

In order to further discuss the computational results, we show in Figs. 2 and 3 the relative difference in the maximum value and the 99th percentile voxel values of the *in-situ* electric field in the whole body phantom. From Fig. 2, the relative differences were within 30% except for those obtained at CRIEPI. By comparing Figs. 2 and 3, the relative differences except for those for CRIEPI are suppressed to several percent for the 99th percentile value. The reason for this difference is attributed to the singular behavior of the edge of the voxels in the discretized phantom [28].

We also show in Fig. 4 the relative differences in the 99th-percentile voxel value of the *in-situ* electric field in the CNS. The relative differences for the CNS are comparable but somewhat larger than those of the whole body, presumably because the nerve tissues are surrounded by cerebrospinal fluid, which has a large conductivity relative to that of CNS tissues. The high contrast of tissue conductivity may lead to larger computational uncertainty as reported in [28].

We show in Fig. 5 the relative difference in the maximum voxel value of the current density in the body phantom. By comparing Figs. 2 and 5, the relative difference in the current density of CRIEPI becomes suppressed as compared with that for the *in-situ* electric field. This difference could be caused by the difference in the tissues where the maximal value appears. The maximal current density appears in the CSF, which has the highest conductivity, while the maximal value of the electric field appears around the body surface, which may include some singular behavior due to the stair-casing approximation of the body.

We show in Fig. 6 the relative difference in the maximum current densities averaged over an area of  $1 \text{ cm}^2$  for all tissues. By comparing Figs. 5 and 6, the relative differences in the maximal value of current density averaged over  $1 \text{ cm}^2$  are somewhat smaller than those for the voxel-maximal current density. However, no clear tendency was observed from the comparison of these figures. The reason for this could be that the current density averaged over a specific area largely depends on the tissue inhomogeneity.

We show in Fig. 7 the relative difference in the maximum current density averaged over an area of  $1 \text{ cm}^2$  of the CNS. By comparing Figs. 6 and 7, the relative difference in the maximal value of current density averaged over  $1 \text{ cm}^2$  for the nerve tissue is smaller than that for the whole-body phantom. Except for the results at TNCT, the relative difference in most cases is generally smaller than 10%.

Here it is worth comparing our intercomparison with previous studies. In [8], the frequency region considered is the same as in the present study. The difference in *in-situ* electric field/current density reported in [8] diverged from a few (minimum) to more than a hundred percent (maximum) even for organ-average quantities. Differences larger than those shown the present study are attributed to the effect of conductivities and the human body phantom, even though they are set identically in the present study to focus on the computational uncertainty. Intercomparison of radio-frequency whole-body exposures, has been conducted by three groups [29]. The measure was the whole-body averaged specific power absorption rate, or the total power absorbed by the human phantom. The difference among the three groups was up to several percent, even for the same human phantom and conductivities. Our comparison in the maximum value of the current density averaged over an area of  $1 \text{ cm}^2$  for the CNS tissues, which is a metric in the guidelines and a more microscopic measure, was on the order of a few dozen percent, suggesting that the computational uncertainty caused by the computational method could be reasonable.

## CONCLUSION

The present study provides an intercomparison of the *in-situ* electric field and current density in a Japanese adult male model named TARO for uniform magnetic field exposures. A total of six groups have participated in this intercomparison. Except for in-house computational codes developed by the involved groups, the computational conditions were chosen to be identical to focus on the computational uncertainty caused by different computational methods. Reasonable agreement was obtained among the *in-situ* electric fields/current densities calculated by the different groups: Differences in the maximal and 99th percentile value of the *in-situ* electric field were less than 30% and 10% except for the result by one group. In particular, the current density averaged over  $1 \text{ cm}^2$  for CNS tissue, which is a metric for human protection [1], is 10% or less except for the result by one group. This comparison suggests that computational uncertainty in the induced current and the *in-situ* electric field due to different methods and coding is relatively smaller than that caused by different models and conductivities of tissues, which was reported in a previous study [8].

## ACKNOWLEDGEMENTS

This intercomparison has been conducted under the auspices of the Investigation Committee on Non-uniform and Transient Electromagnetic Field Exposure on Human, IEE Japan. The authors would like to thank the members of this investigation committee for their discussion and encouragement.

## REFERENCES

1. ICNIRP. Guidelines for limiting exposure to time-varying electric, magnetic and electromagnetic fields (up to 300 GHz) Health Phys. 74, 494-522 (1998).
2. IEEE Std C95.6. IEEE standard for safety levels with respect to human exposure to radio frequency electromagnetic fields, 0–3 kHz. (2002).
3. ICNIRP. Response to questions and comments on ICNIRP guidelines on limiting exposure to time-varying electric, magnetic, and electromagnetic fields (up to 300 GHz). Health Phys. 75, 438-439 (1998).
4. Dawson, T. W. and Stuchly, M. A. High resolution organ dosimetry for human exposure to low frequency magnetic fields. IEEE Trans. Magnet. 34, 1-11 (1998).
5. Gandhi, O. P. and Chen, J-Y. Numerical dosimetry at power-line frequencies using anatomically based models. Bioelectromagnet. Suppl. 1, 43-60 (1992).
6. Dawson, T. W. and Stuchly, M. A. Analytic validation of a three-dimensional scalar-potential finite-difference code for low-frequency magnetic induction. Appl. Comput. Electromagnet. Soc. J. 11, 63-71 (1996).
7. Dawson, T. W. and Stuchly, M. A. Effects of skeletal muscle anisotropy on human organ dosimetry under 60 Hz

- uniform magnetic field exposure. *Phys. Med. Biol.* 43, 1059-1074 (1998).
8. Stuchly, M. A. and Gandhi, O. P. Inter-laboratory comparison of numerical dosimetry for human exposure to 60 Hz electric and magnetic fields. *Bioelectromagnet.* 21, 167-174 (2000).
9. Dimbylow, P. J. Induced current densities from low-frequency magnetic fields in a 2 mm resolution, anatomically realistic model of the body. *Phys. Med. Biol.* 43, 221-230 (1998).
10. Yamazaki, K. Current status of studies on estimation of induced currents in a human body exposed to ELF magnetic field. *Proc. of 2008 IEEE Annual Conf.*, H1-5 (2008) (in Japanese).
11. Tarao, H. Hayashi, N. and Isaka, K. Numerical analysis of induced currents in human head exposed to nonuniform magnetic field including harmonics. *IEEE Trans. on FM.* 123, 1100-1107 (2003).
12. Dimbylow, P. Development of the female voxel phantom, NAOMI, and its application to calculations of induced current densities and electric fields from applied low frequency magnetic and electric fields. *Phys. Med. Biol.* 50, 1047-1070 (2005).
13. Hamada, S. and Kobayashi, T. Analysis of electric field induced by ELF magnetic field utilizing fast-multipole surface-charge-simulation method for voxel data. *IEEE Trans. FM*, 126 355-362 (2006) (in Japanese).
14. Kamimura, Y. Ito, K. and Yamada, Y. Calculation of induced current inside a human body near an IH cooker by SPFD method. *Int'l Workshop on Biological Effects of EMFs*, 970-974 (2006).
15. Leitgeb, N. and Cech, R. Dosimetric assessment of simultaneous exposure to ELF electric and magnetic fields *IEEE Trans. Biomed. Eng.* 55, 671-674 (2008).
16. Maruyama, K. Suzuki, Y. Taki, M. Wake, K. Watanabe, S. and Hashimoto, O. Coupling characteristic of adult and children with non-uniform magnetic field. *Proc. XXIX URSI General Assembly, KAE.2* (2008).
17. Yamazaki, K. Kawamoto, T. Fujinami, H. and Shigemitsu, T. On the method of investigating human exposure to nonuniform magnetic field *Electrical Eng. Jpn.* 164, 1-11 (2008).
18. Hirata, A. Wake, K. Watanabe, S. and Taki, M. In-situ electric field and current density in Japanese male and female models for a uniform magnetic field exposures *Rad. Prot. Dosimetry.* 135, 272-275 (2009).
19. WHO. Environmental Health Criteria 238: Extremely low Frequency (ELF) Fields WHO (Geneva, Switzerland) (2007).
20. Nagaoka, T. Watanabe, S. Sakurai, K. Kunieda, E. Watanabe, S. Taki, M. and Yamanaka, Y. Development of realistic high-resolution whole-body voxel models of Japanese adult males and females of average height and weight, and application of models to radio-frequency electromagnetic-field dosimetry. *Phys. Med. Biol.* 49, 1-15 (2004).
21. Gabriel, S. Lau, R. W. and Gabriel, C. The dielectric properties of biological tissues: III. Parametric models for the dielectric spectrum of tissues *Phys. Med. Biol.* 41, 2271-293 (1996).
22. Orcutt, N. and Gandhi, O. P. A 3D impedance method to calculate power deposition in biological bodies subjected to time varying magnetic fields *IEEE Trans. Biomed. Eng.* 35, 577-583 (1998).
23. De Moerloose, J. Dawson, T. W. and Stuchly, M. A. Application of finite difference time domain algorithm to quasi-static field analysis *Radio Sci.* 32, 329-341 (1997).
24. IEEE, Technical Report of Investigation Committee on Electric Field and Current Induced in a Human Body Exposed to Electromagnetic Fields: Calculation of electric field and current induced in a human body exposed to electromagnetic fields, no.1067 (2006) (in Japanese)
25. Greengard, L. and Rokhlin, V. A new version of the Fast Multipole Method for the Laplace equation in three dimensions. *Acta Numerica.* 6, 229-269 (1997).
26. Hirata, A. and Fujiwara, O. Dosimetry in Japanese male and female models for low-frequency electric field. *Phys. Med. Biol.* 52 N339-N343 (2007).
27. ICNIRP. Response to CENELEC Working Group Convener. CENELEC TC106X online document archive, Document TC106X/Chair/0006/INF (1999).
28. Dawson, T. W. Potter, M. E. and Stuchly, M. A. Evaluation of the modeling accuracy of power frequency field interactions with the human body *Appl. Comput. Electromagnet. Soc. J.* 16, 162-172 (2001).
29. Dimbylow, P. Hirata, A. and Nagaoka, T. Intercomparison of whole-body averaged SAR in European and Japanese voxel phantoms. *Phys. Med. Biol.* 53, 5883-5897 (2008).

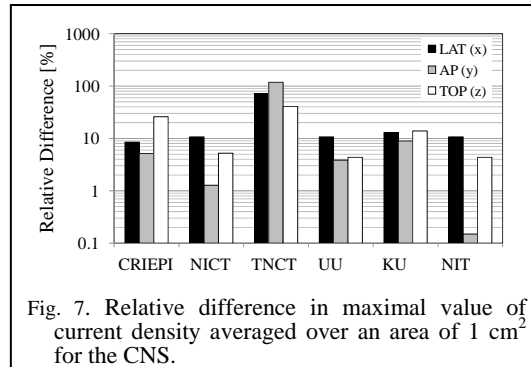
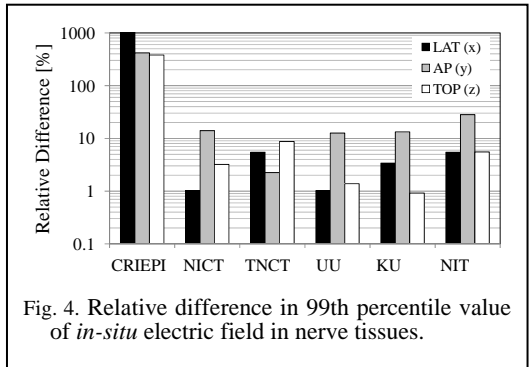
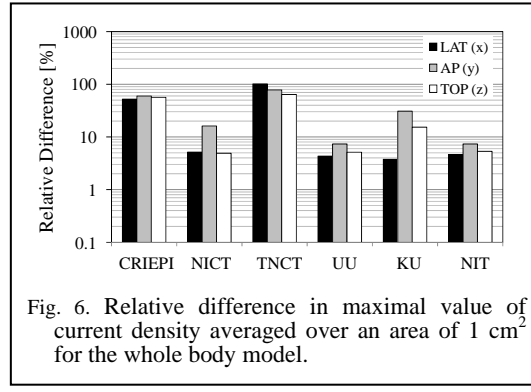
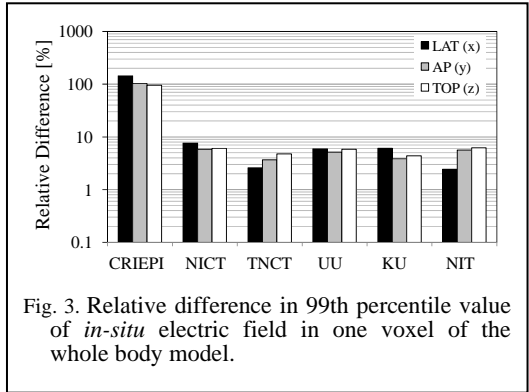
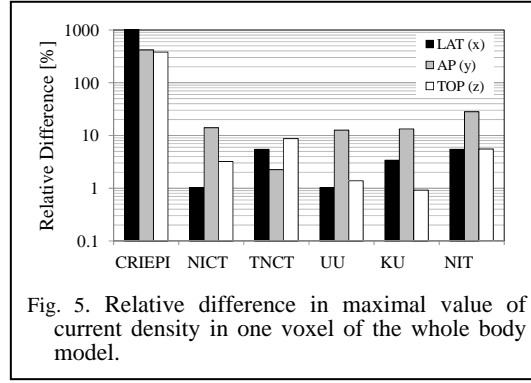
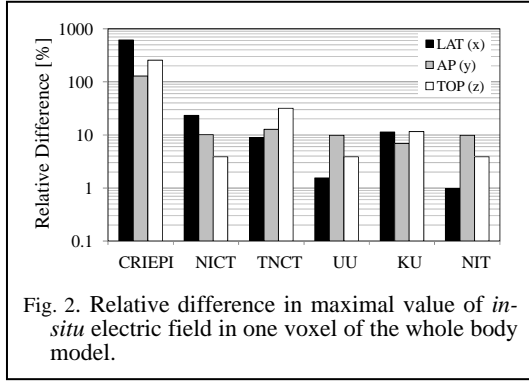


Table 2. *In-situ* electric field and induced current density in humans for magnetic field exposure. C.S.F represents cerebrospinal fluid.

X LAT	CRIEPI		NICT		Taka Tech		Utsunomiya Univ.		Kyoto Univ.		NIT	
	values	tissues	values	tissues	values	tissues	values	tissues	values	tissues	values	tissues
(i)	128	cortical bone	13.7	cortical bone	16.3	cortical bone	17.6	cortical bone	19.9	cortical bone	17.7	cartilage
(ii)	8.70		3.30		3.48		3.36		3.79		3.66	
(iii)	44.1	spinal cord	2.90	gray matter	3.09	spinal cord	2.90	white matter	2.83	gray matter	2.77	gray matter
(iv)	3.72	CSF	7.39	CSF	15.7	CSF	8.13	CSF	7.50	CSF	8.15	CSF
(v)	2.59	CSF	2.40	CSF	3.75	CSF	2.41	CSF	1.97	CSF	2.42	CSF
(vi)	1.85	spinal cord	2.24	spinal cord	3.48	spinal cord	2.24	spinal cord	1.76	spinal cord	2.24	spinal cord

Y AP	CRIEPI		NiCT		Taka Tech		Utsunomiya Univ.		Kyoto Univ.		NIT	
	values	tissues	values	tissues	values	tissues	values	tissues	values	tissues	values	tissues
(i)	79.3	cortical bone	31.1	skin	39.0	skin	31.2	skin	37.0	skin	31.2	skin
(ii)	12.4		5.76		5.89		5.80		6.35		6.46	
(iii)	15.0	spinal cord	2.49		2.83	spinal cord	2.53	gray matter	2.51	white matter	3.71	spinal cord
(iv)	2.80	muscle	8.09	CSF	12.4	CSF	7.48	CSF	4.81	CSF	7.48	CSF
(v)	1.88	CSF	4.07	CSF	4.27	CSF	4.10	small intestine	3.20	small intestine	1.70	CSF
(vi)	1.64	gray matter	1.54	spinal cord	3.40	spinal cord	1.50	gray matter	1.42	gray matter	1.56	gray matter

Z TOP	CRIEPI		NiCT		Taka Tech		Utsunomiya Univ.		Kyoto Univ.		NIT	
	values	tissues	values	tissues	values	tissues	values	tissues	values	tissues	values	tissues
(i)	60.0	cortical bone	16.2	fat	11.5	fat	16.2	fat	18.8	fat	16.2	fat
(ii)	7.50		3.60		3.65		3.61		4.00		4.07	
(iii)	10.4	spinal cord	2.10		1.98	white matter	2.14	gray matter	2.15	white matter	2.29	gray matter
(iv)	2.10	CSF	5.07	CSF	7.93	CSF	5.08	CSF	4.09	CSF	5.09	CSF
(v)	1.52	CSF	2.03	CSF	2.23	CSF	1.40	muscle	1.42	muscle	1.30	CSF
(vi)	1.46	gray matter	1.22	gray matter	1.63	white matter	1.21	gray matter	1.00	gray matter	1.21	gray matter